JACS
JOURNAL OF THE AMERICAN CHEMICAL SOCIETY
Article
pubs.acs.org/JACS

On the Influence of Water on the Electronic Structure of Firefly Oxyluciferin Anions from Absorption Spectroscopy of Bare and Monohydrated Ions in Vacuo

Kristian Støchkel,[†] Christian Nygaard Hansen,[†] Jørgen Houmøller,[†] Lisbeth Munksgaard Nielsen,[†] Kelvin Anggara,[†] Mathieu Linares,[‡] Patrick Norman,[‡] Fernando Nogueira,[§] Oleg V. Maltsev,[∥] Lukas Hintermann,[∥] Steen Brøndsted Nielsen,*[,†] Panče Naumov,*[,⊥,#] and Bruce F. Milne*[,§]

[†]Department of Physics and Astronomy, Aarhus University, Ny Munkegade, DK-8000 Aarhus C, Denmark

[‡]Division of Computational Physics, Department of Physics, Chemistry and Biology (IFM), Linköping University, SE-581 83 Linköping, Sweden

[§]Centre for Computational Physics, Department of Physics, University of Coimbra, Rua Larga, 3004-516 Coimbra, Portugal

[∥]Department Chemie, Technische Universität München, Lichtenbergstrasse 4, 85748 Garching bei München, Germany

[⊥]New York University Abu Dhabi, P.O. Box 129188, Abu Dhabi, United Arab Emirates

[#]Institute for Chemical Research and the Hakubi Center for Advanced Research, Kyoto University, Uji, Kyoto 611-0011, Japan

Supporting Information

ABSTRACT: A complete understanding of the physics underlying the varied colors of firefly bioluminescence remains elusive because it is difficult to disentangle different enzyme–lumophore interactions. Experiments on isolated ions are useful to establish a proper reference when there are no microenvironmental perturbations. Here, we use action spectroscopy to compare the absorption by the firefly oxyluciferin lumophore isolated in vacuo and complexed with a single water molecule. While the process relevant to bioluminescence within the luciferase cavity is light emission, the absorption data presented here provide a unique insight into how the electronic states of oxyluciferin are altered by microenvironmental perturbations. For the bare ion we observe broad absorption with a maximum at 548 ± 10 nm, and addition of a water molecule is found to blue-shift the absorption by approximately 50 nm (0.23 eV). Test calculations at various levels of theory uniformly predict a blue-shift in absorption caused by a single water molecule, but are only qualitatively in agreement with experiment highlighting limitations in what can be expected from methods commonly used in studies on oxyluciferin. Combined molecular dynamics simulations and time-dependent density functional theory calculations closely reproduce the broad experimental peaks and also indicate that the preferred binding site for the water molecule is the phenolate oxygen of the anion. Predicting the effects of microenvironmental interactions on the electronic structure of the oxyluciferin anion with high accuracy is a nontrivial task for theory, and our experimental results therefore serve as important benchmarks for future calculations.

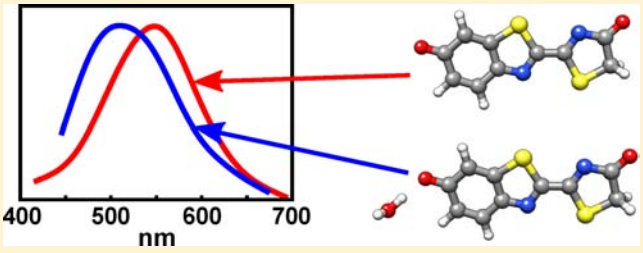

INTRODUCTION

Bioluminescent organisms have developed mechanisms for catalytic production of cold light, which they utilize to communicate warning signals, or to attract prey or partners for mating. The core chemical event of bioluminescence (BL) is chemiexcitation, a sequence of chemical reactions, by which ground-state substrates (luciferins) in fireflies[1] and some coelenterates[2] are enzymatically converted by luciferase (**Luc**) to energy-rich intermediates. The intermediates, bearing a labile dioxetanone moiety in fireflies,[3] decompose to produce the first excited state of the emitters, oxyluciferins, which relax to the ground state by emitting a photon of visible light.[4] The one-to-one ratio of molecules of the intermediate and photons in this last step renders the BL reaction a very efficient process, with quantum yields that largely exceed those observed with non-natural chemiluminescence reactions.[4] The efficient BL emission can be utilized in microbiological analysis[5] and is currently an indispensable tool in multicolor in vivo imaging.[6−8] Recently, the potentials for applications involving secondary energy-transfer processes have been realized, including BRET in luciferase–protein dyads,[9] FRET-based imaging with enzyme–quantum dot conjugates,[10,11] and sequential energy transfer (BRET-FRET).[12]

The utility of BL as imaging tool triggered a great deal of research with the goal of developing an understanding of the underlying mechanisms. The dioxetanone intermediate in the firefly BL reaction sequence is an extremely unstable species

Received: November 20, 2012
Published: April 4, 2013

   dx.doi.org/10.1021/ja311400t | J. Am. Chem. Soc. 2013, 135, 6485−6493

that remains synthetically inaccessible. Under controlled conditions, the lumophore ($\mathbf{OxyLH_2}$) can be stabilized in the ground state for a reasonably long time, but the ground-state structure does not provide direct insight into the excited-state dynamics.[13−15] A large number of theoretical studies have also been performed with the aim of elucidating details of the factors controlling BL (for recent reviews, see Navizet (2011),[16] Hosseinkhani (2011),[17] and da Silva (2011)[18]). These studies have increased in complexity since initial gas-phase calculations and now routinely include solvent effects, either implicitly through the use of continuum dielectric models, or by explicit inclusion of solvent molecules[19,20] (the results of Min et al.[20] relate directly to the excited state of oxyluciferin) and even reduced models of the luciferase microenvironment;[21−24] the spectrochemistry of $\mathbf{OxyLH_2}$ has been experimentally established only in neat solutions.[14,15] Most theoretical considerations of the effects of the luciferase framework are limited to the relevant amino acid residues from the crystal structures of luciferases from *Luciola cruciata*[25] or *Photinus pyralis*.[26] Recent results, however, suggest significant reorganization of the microenvironment during the lumophore deexcitation, thus questioning some earlier mechanistic inferences based on the ground-state structure of the luciferase−oxyluciferin complex, $[(\mathbf{Luc})(\mathbf{OxyLH_2})]$.[24]

Unlike fireflies (Lampyridae), which communicate the characteristic bursts of yellow-green light, and despite the fact that they utilize identical lumophore, some species of click beetles (Elateridae) emit orange light, while certain railroad worm species (Phengodidae) luminesce in the red region. These shifts in the emission color were successfully mimicked by deliberate point mutations in the Lampyridae luciferase family, and the wavelength of emission can be artificially tuned to values between 530 and 640 nm. As many as six mechanisms have been advanced to explain the molecular origin of this phenomenon, although without a consensus on its origin. The suggested mechanisms include keto−enol tautomerization, molecular twisting in excited state, effects of microenvironment (including deprotonation of the phenol functionality) and tautomerization/deprotonation of the hydroxythiazole fragment, stabilization by charge resonance, conformational changes in the active pocket, and concomitant modulation of polarity and covalency of an emitter−cation ion-pair. Experimental and theoretical contra-arguments have been subsequently advanced that discredit each of these mechanisms. Despite the numerous attempts and various experimental and theoretical approaches, due to lack of photophysical data on the excited lumophore free from environment effects, this conundrum remains unresolved.

A direct experimental spectrochemical benchmark of a single excited molecule $(\mathbf{OxyLH_2})^*$ in vacuo could end the long-term dispute. Indeed, the spectrochemical effects from the environment exerted by the amino acid residues or water molecules in the luciferase active pocket could be directly assessed against the spectral fingerprint of the bare ion if the latter were to be isolated in the absence of intermolecular interactions. This approach represents a simple, yet critically important starting point to understand the true reasons behind the color tuning and is the one we have taken here to shed light on this problem. Computational studies have previously highlighted the importance of water molecules in the firefly oxyluciferin system,[23,27,28] and it was recently proposed[14] that a single water molecule in the protein cavity could have a profound effect on the photophysical properties of the emitter and its dynamics. Theoretical investigations of interactions between oxyluciferin and components of the luciferase active site in available crystal structures support the importance of water molecules in terms of their energetic effect on the emitter.[18,27] To verify this hypothesis, using a special experimental setup, we utilize here action spectroscopy of the ionized firefly emitter $\mathbf{OxyLH^-}$ and its ion-complex $[(\mathbf{OxyLH})(\mathbf{H_2O})]^-$ to elucidate the spectrochemical consequences of a single water molecule on the isolated ion in vacuo. The 5,5-dimethyloxyluciferin anion ($\mathbf{DMOxyL^-}$) was also included to provide a color-shift standard free of the potential variability of the gas phase $[(\mathbf{OxyLH})(\mathbf{H_2O})]^-$ complex. Finally, we note that recent theoretical work by Navizet et al.[29] supports the use of the isolated oxyluciferinate anion as a model for the firefly lumophore because their results indicate that the light emitter is the same after chemical decomposition of firefly dioxetanone (either in vacuo or within the protein) to that obtained after photoexcitation of oxyluciferin.

In our experiment, we probe absorption and not light emission because the ion density is too low to result in enough emitted photons for detection. Indeed, the ion density is also insufficient for conventional light transmission experiments that are normally used to obtain absorption spectra, and this constitutes a significant barrier to the measurement of absorption by ions in vacuo. Instead, gas-phase ion spectroscopy relies on ionic dissociation driven by light absorption. In our setup, such action spectroscopy on macromolecular ions is realized by combining an electrospray ion source, electrostatic ion storage ring, and pulsed lasers. The setup has already provided valuable information on the light absorption by several chromophore ions, ionic GFP chromophore, protonated retinal Schiff bases, heme, porphyrin, and peptides,[30−35] and the bioluminescence precursor, the D-(−)-luciferinate anion, $\mathbf{LH^-}$.[36] Recently, we have also modified an accelerator mass spectrometer (sector instrument) to perform gas-phase spectroscopy experiments. While delayed dissociation on time scales of hundreds of microseconds to tens of milliseconds is monitored in the ring experiment, fast dissociation occurring within a few microseconds is probed by the accelerator mass spectrometer. These complementary techniques were employed here to record the action spectra of isolated anions of $\mathbf{OxyLH_2}$ and its complex with a single water molecule. These ground-state absorption data are indispensable direct benchmarks against which the theoretical models commonly used in studies of the excited-state structure of the firefly emitter can be assessed for the first time free from interferences by the complex structure of the luciferase active site. If such models can correctly predict the absorption by oxyluciferin and the influence of a microenvironment, they are likely also capable of providing useful information regarding microenvironmental effects in the emission spectra.

RESULTS AND DISCUSSION

Isolated $\mathbf{OxyLH^-}$ and $\mathbf{DMOxyL^-}$ Anions. First, we present the results from the storage ring experiments, where neutrals produced as a result of dissociation are monitored as a function of time. Time spectra obtained after photoexcitation in the ring of the $\mathbf{OxyLH^-}$ ion (m/z = 249) at 490, 530, and 580 nm, shown in Figure 1, confirm that the photoinduced dissociation is nearly complete after 400 μs. This time is much shorter than the storage time in the ring (~0.3 s). The revolution time of the ions is 64 μs. The neutrals that gave rise to the count rate were produced ~19 μs after the photo-

dx.doi.org/10.1021/ja311400t | J. Am. Chem. Soc. 2013, 135, 6485−6493

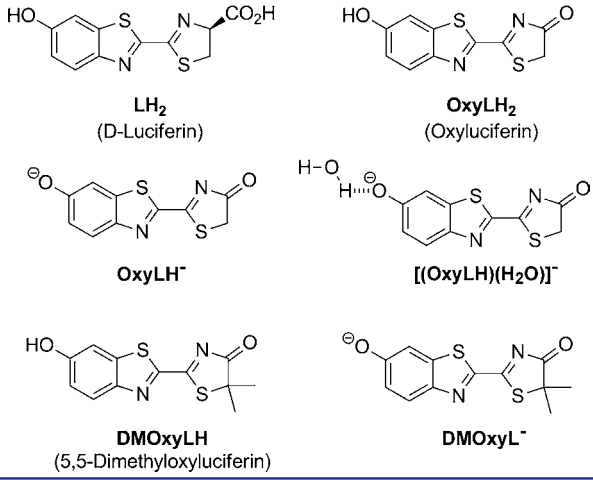

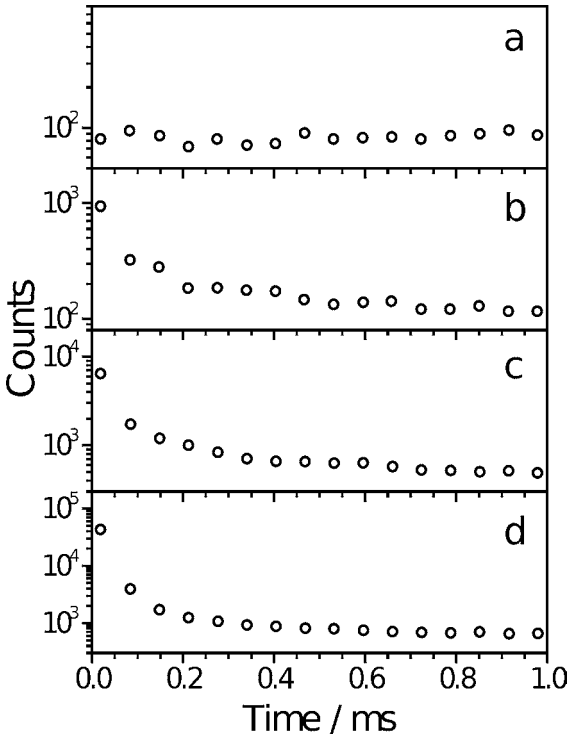

Figure 1. Time spectra of oxyluciferinate anions without laser irradiation (a), and after photoexcitation at 490 nm (b), 530 nm (c), and 580 nm (d). The spectrum in panel (a) is due to neutrals formed after collisions between the ions and the residual gas in the ring.

excitation in the first instance (first point in the time spectrum), and then after successive rotations in the ring. According to a power dependence study, the first point is due to neutrals formed from ions that have either absorbed one or two photons, whereas the following points are due to one-photon absorption. The contribution of the two-photon absorption to the first point increases with wavelength because lower excitation energies allow more ions to survive the travel from the laser-irradiated region to the opposite side of the ring where their decay is sampled. At high laser powers, the photoyield of neutrals saturates. To avoid such saturation effects and to minimize two-photon absorption, the power was attenuated during wavelength scans, and the first point was not included in the analysis. The subsequent five points were summed excluding the background of neutrals formed as a result of collisions with residual gas in the ring (see Figure 1a). The yield of photoneutrals was then divided by the background count to correct for variations in the ion beam intensity and the number of photons in the laser pulse. This action signal is taken to represent the relative absorption cross section. Figure 2a shows the cross sections versus wavelength. The spectrum displays a broad band with λ_{max} between 535 and 555 nm with fwhm (full width at half maximum) of 95 nm.

Next, we consider the results from the single-pass experiments with the accelerator mass spectrometer. Here, ionic fragments formed up to 3 μs after photoexcitation were sampled, in contrast to the storage ring experiment where delayed dissociation was monitored on a much longer time scale. Photoexcitation leads to one dominant fragment anion at m/z = 175 and a minor one at m/z = 206 that correspond to loss of C_2H_2SO (mass 74) and C_2H_3O (mass 43), respectively. These are both formed as a result of two-photon absorption, in agreement with the time-spectra discussed above (the one-photon absorption is excluded in this experiment based on the narrow temporal window for dissociation). We assign the m/z = 175 fragment to deprotonated 2-cyano-6-hydroxybenzothiazole. Interestingly, this molecule is a breakdown product in the reactions between the oxyluciferin and water within the enzyme cavity required for repetitive flashing of the firefly emission.[37]

The yields of each of the two fragment ions were measured as a function of the wavelength to give action spectra after correcting for ion beam fluctuations and number of photons in the laser pulses. The action spectrum based on the m/z = 175 fragment ion (Figure 2b) is similar to that obtained from the ring experiment: It displays a broad band with λ_{max} between 540 and 560 nm (Figure 2a). The spectrum based on the m/z = 206 ion (not shown) is similar but of worse quality due to much lower ion yields. Taken together, the results show that the bare oxyluciferinate anion **OxyLH**$^-$ absorbs maximally at 548 ± 10 nm, and that the absorption spectrum is broad (fwhm of 95 nm). We note that the absorption band of **OxyLH**$^-$ is only slightly red-shifted as compared to that of **LH**$^-$ (532 nm) reported earlier[36] despite the greater electron delocalization expected in the former. The excess electron density in **OxyLH**$^-$ can be located at either oxygen (two limiting resonance structures), while the carboxylate group in **LH**$^-$ is not conjugated with the ring π-electrons.

According to our calculations, the dominant tautomer of the oxyluciferinate ions isolated in our ion beam at room temperature is the keto form. As discussed later, the agreement between the predicted and the measured absorption bands is in strong support of this assignment. To ascertain the tautomer identity, the measurements were repeated with the 5,5-dimethylated oxyluciferinate anion (**DMOxyL**$^-$ m/z = 277) where the molecule is locked as the keto tautomer by substitution. The action spectrum obtained based on the m/z = 175 fragment ion has a λ_{max} = 540−570 nm (Figure 2d), while the ring experiment provides λ_{max} = 560−580 nm (Figure 2c). Our estimate of the band maximum is 565 ± 10 nm. The red-shift of about 17 nm relative to **OxyLH**$^-$ is in accordance with the substitution effects observed in solution.[14] The calculated spectra described below confirm that this spectral shift is due to substitution effects.

[(OxyLH)(H$_2$O)]$^-$ Complex Anion. The impact of a single water molecule on the electronic structure of oxyluciferinate anions was measured with the accelerator mass spectrometer. While the photoinduced dissociation mass spectrum of bare **OxyLH**$^-$ was rather simple with two important fragment ions,

dx.doi.org/10.1021/ja311400t | J. Am. Chem. Soc. 2013, 135, 6485−6493

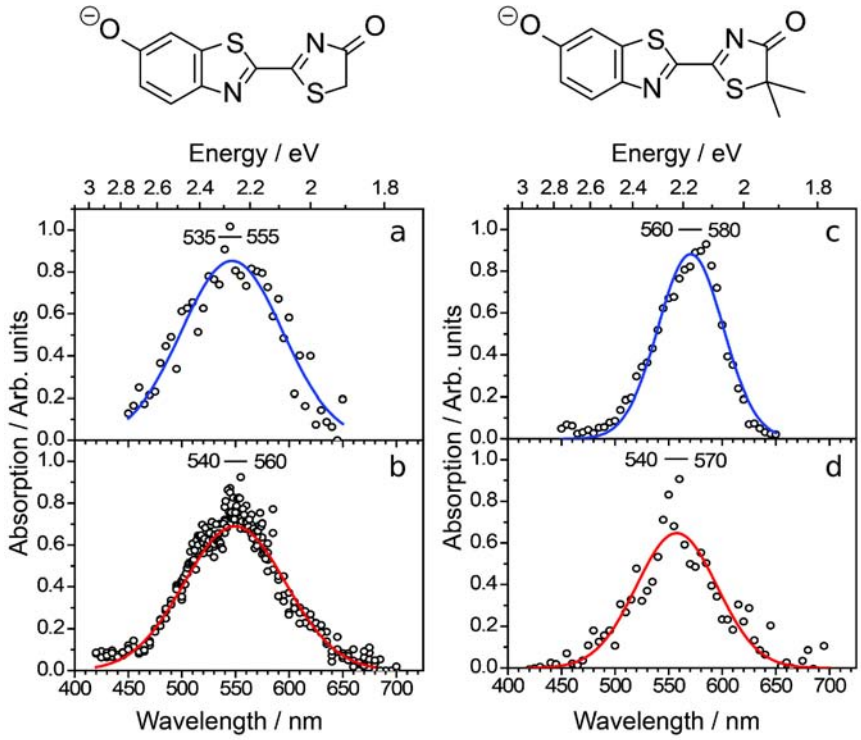

Figure 2. Action spectra of oxyluciferinate and 5,5-dimethyloxyluciferinate anions obtained using two different instruments. **OxyLH**$^-$: (a) ELISA, sampling of neutral fragments; (b) accelerator mass spectrometer, sampling of m/z = 175 fragment ions. **DMOxyL**$^-$: (c) ELISA, sampling of neutral fragments; (d) accelerator mass spectrometer, sampling of m/z = 175 fragment ions. In the ELISA experiment, we detect neutrals traveling with high kinetic energies as they deposit energy in the detector, but we have no mass information. The curves are Gaussian fits to the data.

many more dissociation channels are available for the $[(\mathbf{OxyLH})(\mathbf{H_2O})]^-$ complex, including water loss, dissociation of the bridge between the two heterocycles, and decomposition of one of the rings. The water molecule remained bound to several fragment ions. The dominant fragment ion had m/z = 150 and is ascribed to separation of the two heterocyclic rings. The action spectra of each of the fragment ions are shown in Figure 3 (insufficient background counts from collision-induced dissociations prevented us from applying spectral corrections for ion beam fluctuations). The count rates of the photo-induced fragment ions were typically 1 s^{-1}, which placed a practical burden on this experiment. Nevertheless, the spectra are quite similar with λ_{max} = 480−530 nm. The minor differences may be related to the different structures of the oxyluciferinate−water complexes in the ion beam that could result in different dissociation pathways. Regardless of these small differences, the spectra are conclusive that a water molecule blue-shifts the absorption of the ion.

Theoretical Results. The optimized ground-state geometries used in all calculations are shown in Figure 4. Details of the optimization strategies and relative energies for different conformational and configurational properties are dealt with in the Methods section. These geometries were used for the evaluation of several common methods for the calculation of vertical electronic excitation energies.

The results of single-point EOM-CCSD and TDDFT electronic absorption calculations are given in Table 1. With the EOM-CCSD/Def2-TZVPPD method, a value of 481 nm was obtained for the **OxyLH**$^-$ excitation wavelength, as compared to the experimental wavelength of 548 ± 10 nm. At the EOM-CCSD level with the smaller Def2-SVPD basis set, these values were red-shifted by only ∼0.01 eV, indicating that the smaller basis set was capable of producing well-converged results.

The reduced excitation level (REL) diagnostic gives a measure of the character of a given excitation within the EOM-CC framework. Values close to unity indicate predominantly single-excitation character, while higher values indicate multiexcitation character. In all calculations performed in the present work, the excitations had REL values of 1.1 ± 0.02. Therefore, the excitations observed in the oxyluciferin systems possess predominantly single-excitation character, and all of the relevant physics should be described accurately even with the truncation of the coupled-cluster expansion at second order.[38] Greater multielectron character, on the other hand, would have required inclusion of triples excitations, e.g., using EOM-CCSD(T).

Excellent agreement with the high-level EOM-CCSD result came from the two hybrid functionals, B3LYP and CAM-B3LYP, which also showed minimal changes on going from the Def2-SVPD basis set to the much larger Def2-TZVPPD set. However, the pure DFT functionals SVWN and BLYP were found to provide excitation energies that were lower than that obtained with EOM-CCSD and that in fact were in very good agreement with experiment, giving errors for both functionals relative to experiment of less than 10 nm. The fact that the EOM-CCSD and hybrid TDDFT methods gave values that were significantly blue-shifted relative to the experimental **OxyLH**$^-$ value suggested that the approximations used in the calculations were neglecting some effects (e.g., vibronic effects) that were important in the **OxyLH**$^-$ system. The apparently superior performance of the pure DFT functionals was most

dx.doi.org/10.1021/ja311400t | J. Am. Chem. Soc. 2013, 135, 6485−6493

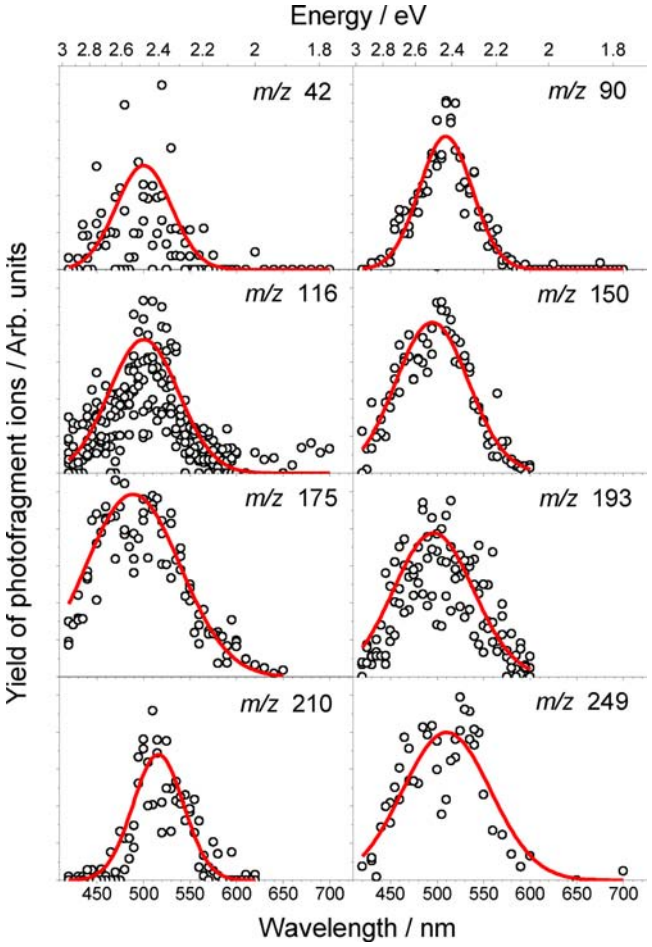

Figure 3. Action spectra of oxyluciferinate–water complexes obtained using the accelerator mass spectrometer. The fragment ion masses are indicated on each panel. The red curves are Gaussian fits to the data.

likely an example of fortuitous cancellation of errors in these formally less sophisticated methods.

In relation to theoretical predictions of color-tuning effects in BL, a more important set of results were the calculated shifts relative to **OxyLH**$^-$ for the $[(\mathbf{OxyLH})(\mathbf{H_2O})]^-$ and **DMOxyL**$^-$ systems (Table 1). The EOM-CCSD/Def2-TZVPPD method yielded a blue-shift of 10 nm for the $[(\mathbf{OxyLH})(\mathbf{H_2O})]^-$ complex and a red-shift of 3 nm for the **DMOxyL**$^-$ anion, which, although providing qualitatively correct predictions, were approximately one-fifth of the size of the shifts observed in the experimental spectra in both cases. Despite the large split between the performance of the pure and hybrid functionals seen in the TDDFT results for **OxyLH**$^-$, there was very little difference in the predicted spectral shifts obtained from the four functionals. All of the TDDFT-predicted shifts for **DMOxyL**$^-$ were ±2 nm relative to EOM-CCSD, while the $[(\mathbf{OxyLH})(\mathbf{H_2O})]^-$ EOM-CCSD shift was underestimated by all of the functionals except CAM-B3LYP, with BLYP performing worst. That all of the methods used here were able to correctly predict the sign of the spectral shift in these systems but failed to deliver the correct magnitude is most likely an indication that the sources of error mentioned above for **OxyLH**$^-$ may become even more critical in these systems due to the complexed water molecule in $[(\mathbf{OxyLH})(\mathbf{H_2O})]^-$ and the addition of two methyl groups in **DMOxyL**$^-$.

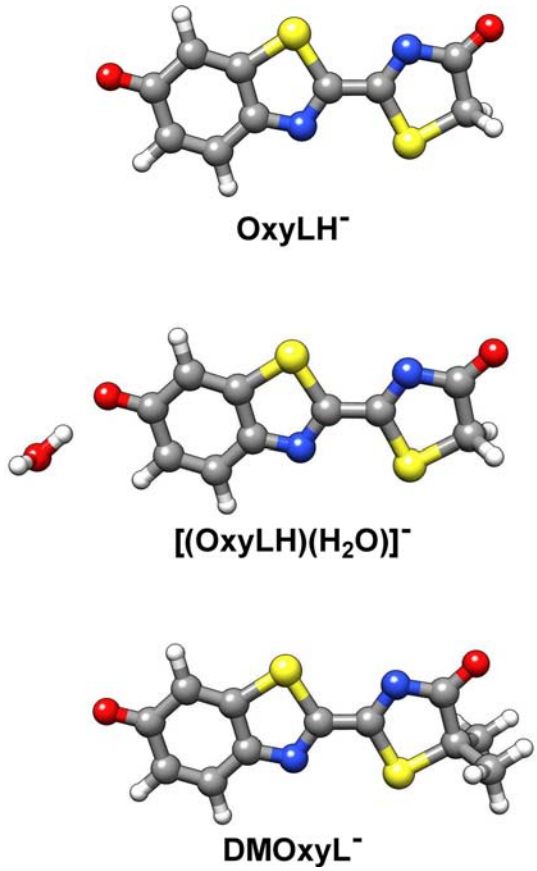

Figure 4. B3LYP/Def2-SVPD optimized structures of the three systems studied.

Table 1. Calculated Absorption Energies for OxyLH$^-$, $[(\mathbf{OxyLH})(\mathbf{H_2O})]^-$, and DMOxyL$^-$[a]

	λ_{abs} ($S_1 \leftarrow S_0$)/nm	
	Def2-SVPD	Def2-TZVPPD
	OxyLH$^-$	
EOM-CCSD	478	477
SVWN	545	546
BLYP	540	542
B3LYP	490	491
CAM-B3LYP	464	466
	$[(\mathbf{OxyLH})(\mathbf{H_2O})]^-$	
EOM-CCSD	470 (−8)	467 (−10)
SVWN	541 (−4)	542 (−4)
BLYP	538 (−2)	539 (−3)
B3LYP	485 (−5)	487 (−4)
CAM-B3LYP	455 (−9)	458 (−8)
	DMOxyL$^-$	
EOM-CCSD	481 (+3)	480 (+3)
SVWN	549 (+4)	550 (+4)
BLYP	544 (+4)	546 (+4)
B3LYP	493 (+3)	495 (+4)
CAM-B3LYP	466 (+2)	469 (+3)

[a]Wavelength shifts relative to isolated **OxyLH**$^-$ given in parentheses.

It is of interest to note that Min et al. performed calculations to investigate the effect of explicit waters on the electronic structure of oxyluciferinate anion at the TD-B3LYP/6-31+G-(d,p)//B3LYP/6-31+G(d,p) level where they found that one water molecule hydrogen-bonded to the phenolate oxygen

dx.doi.org/10.1021/ja311400t | J. Am. Chem. Soc. 2013, 135, 6485−6493

(similar to $[(\mathbf{OxyLH})(\mathbf{H_2O})]^-$ in the present work (Figure 4)) caused a blue-shift of 2 nm in the predicted absorption.[20] The small difference between their blue-shift and our value of 5 nm can be rationalized by the slightly different basis sets used in the geometry optimizations and subsequent excitation calculations. Min et al. included diffuse functions only on non-hydrogens during the geometry optimizations and in the excitation calculations (6-31+G(d,p)), whereas our basis set contained diffuse functions on all atoms (Def2-SVPD).

Min et al. found that when the water molecule was located at the opposite (keto) end of the anion this was found to produce a 4 nm red-shift in the absorption. Thus, longitudinal polarization of the anion in opposite directions was seen to be capable of producing shifts either to higher or to lower energy in the spectrum. This polarization effect was systematically investigated by the incremental application of electric fields during real-space/time TDDFT calculations on the oxyluciferinate anion by Cai et al., who also found that the absorption peak could be shifted either to higher or lower energies by the polarizing field.[39] The redistribution of charge density in the anion due to the electron-withdrawing inductive ($-I$) effect associated with the methyl groups attached to the thiazolone ring in $\mathbf{DMOxyL}^-$ might be expected to be qualitatively similar to the effect of a water molecule hydrogen-bonded to the keto oxygen, which is in keeping with both our experimental and our theoretical data.

A further feature of the experimental spectra that was of interest in terms of the performance of simulation techniques was the significant peak-broadening. In an attempt to extend the single-point static calculations in a way that might shed more light on the origins of this broadening, molecular dynamics (MD) simulations were performed for the three oxyluciferin systems. The resulting composite spectra obtained from TDDFT calculations on the sampled MD trajectories are shown in Figure 5. Both the LDA (SVWN) and the CAM-B3LYP functionals were used, representing the simplest and most complex functionals employed in this study. Although the single-point TD-LDA result for $\mathbf{OxyLH}^-$ was closest to experiment, this was probably due to cancellation of errors at the equilibrium geometry, which might not the case for the distorted geometries obtained from the MD run. TD-CAM-B3LYP performed well relative to the EOM-CCSD data, and its better treatment of charge-transfer type excitations might be important in the distorted geometries.

The spectral profiles obtained from the MD-averaged TD-LDA calculations were found to fit well the degree of band broadening observed experimentally. Differential changes in the band maxima for the three systems enhanced the calculated color shift by 2 nm for both $[(\mathbf{OxyLH})(\mathbf{H_2O})]^-$ and $\mathbf{DMOxyL}^-$ leading to shifts of −6 and +6 nm, respectively, relative to $\mathbf{OxyLH}^-$.

The composite peaks obtained with the CAM-B3LYP functional were slightly less broad than those obtained with LDA. This may be due to a greater sensitivity to geometrical distortion with the LDA functional leading to a greater spread of the excitation energies. The individual excitations are shown in Figure 5 as crosses, and tighter clustering of those obtained with CAM-B3LYP is evident. The peak maxima in the CAM-B3LYP case yielded a blue-shift of 7 nm for $[(\mathbf{OxyLH})(\mathbf{H_2O})]^-$ relative to $\mathbf{OxyLH}^-$, but only a 1 nm red-shift for the $\mathbf{DMOxyL}^-$ anion. These shifts relative to one another are in better proportion for CAM-B3LYP (as compared to the experimental shifts) than with LDA.

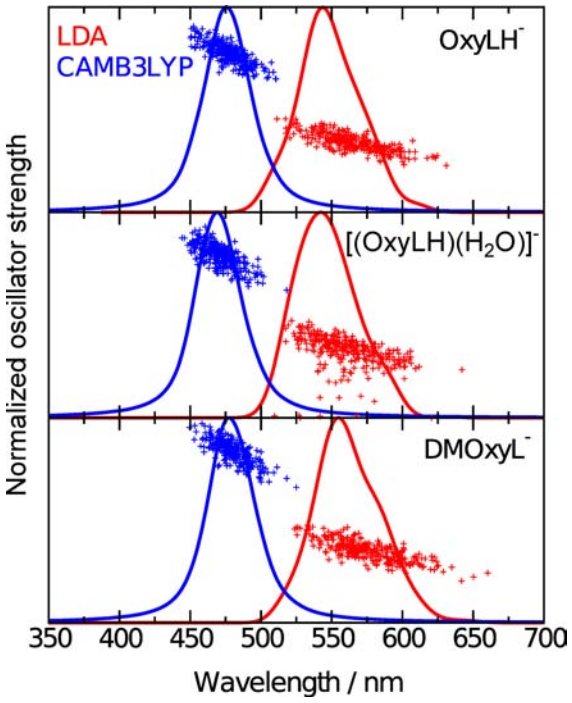

Figure 5. Composite TD-DFT spectra obtained from 300 ps molecular dynamics simulations. Results obtained with the LDA (SVWN) functional are shown in red, and those obtained with the CAM-B3LYP functional are shown in blue. Spectral profiles were obtained from sums of Lorentzian functions fit to individual excitations (+), which were then normalized to put them on the same scale as the single excitations.

It is interesting to note that during the MD simulations the maximum deviation from planarity of the oxyluciferins was of the order of 10−20° in agreement with the DFT calculations and confirming the quality of the force field parametrization (a plot of the energy of rotation about the inter-ring carbon−carbon bond in $\mathbf{OxyLH}^-$ is shown in Figure S2). These data provided further evidence that only the low energy trans-form should be populated at room temperature, in agreement with the Boltzmann factor ratio given below (Methods section). During the simulation started with the water molecule located at the phenolate end of oxyluciferin, the water was seen to migrate to the benzothiazole nitrogen in ∼10% of the snapshots where the absorption was red-shifted to ∼590 nm. However, the small percentage of snapshots where this occurred combined with the fact that the oscillator strengths for the excitation were lower than the average during the simulation meant that this had a small effect on the overall spectrum. Repeat simulations with the water molecule located initially at the midpoint of the oxyluciferin or bound to the keto oxygen were run, but in these cases the water rapidly migrated to the phenolate group and remained there as was seen in the first simulation.

Relation of Gas-Phase Data to Firefly Bioluminescence. All Lampyridae species naturally emit green-yellow light, although at slightly different wavelengths. A consistent property of the spatial disposition of the amino acids in the active pocket of their luciferases is a "barrel" of low polarity, which wraps the substrate/product, with the two termini being exposed to polar environments. This provides a central microenvironment with properties more comparable to the gas phase than to bulk (aqueous) solvent. *Photuris pennsylvanica*

dx.doi.org/10.1021/ja311400t | *J. Am. Chem. Soc.* 2013, 135, 6485−6493

fireflies emit green light with a maximum at λ_{max}^{em} = 538 nm, while the North American fireflies *Photinus pyralis* produce yellow-green light at λ_{max}^{em} = 562 nm. Although they share a significant portion of the **Luc** amino acid sequence with fireflies, the railroad worms *Phrixotrix hirtus* produce red light with λ_{max}^{em} = 623 nm. For the bare ion, we observe broad absorption with a maximum at λ_{max}^{abs} = 548 ± 10 nm. The typical Stokes shifts of oxyluciferin in nonaqueous diluted solutions, as a very crude estimate for the respective gas-phase values, range between 69 and 96 nm, with the values in solvents of low polarity being at the higher end of this range.[14] As the absorption sets a lower limit for the wavelength of emitted light, the estimated emission of the bare ion at 617−644 nm (orange or red) necessitates inclusion of microenvironment effects to account for the natural emission at lower wavelengths (green). Indeed, the action spectra recorded here evidenced that addition of a single water molecule blue-shifts the absorption by about 50 nm. A single water molecule could blue-shift the Stokes-shifted emission of the ion in vacuo to about 567−594 nm (i.e., green to yellow). The results of the present study suggest that such a dynamic water molecule could make a significant contribution to shifting the emission color of the oxyluciferinate ion between green and red. Further support for this suggestion can be found in the results of molecular dynamics simulations of oxyluciferin in which the importance of water molecules in modulating electronic structure in the ground and excited states in the enzyme active site was highlighted.[28,29]

The crystal structure of the complex of *Luciola cruciata* luciferase with oxyluciferin does not contain a water molecule bound to the phenoxyl group of the lumophore.[25] Several waters are located nearby, but these are presumably strongly constrained in the electrostatic environment of the pair of arginine residues at the benzothiazole end of the active site. However, the benzothiazole hydroxyl group in structures of both wild-type and mutant luciferases in a complex with a molecule that represents a model for the unstable intermediate in the bioluminescence reaction is bound to a water molecule at 2.7 Å from the oxygen atom.[25] Combined with the molecular dynamics results mentioned above[28,29] and the results of the present work, this observation appears to support our proposal that a dynamic water molecule could interact significantly with the benzothiazole oxygen of oxyluciferin and may play an important role in the color tuning of the firefly emission.

Another issue to consider is that the most favorable location of the water may be different in the excited state than in the ground state of the oxyluciferin anion. Because, in the biological setting, the oxyluciferin anion is formed in its excited state, it is possible that the water is located in a way that it stabilizes the excited state more than the ground state. As a result, the water molecule would then cause a red-shifted emission. In accordance with this, Ai-min and co-workers[20] predicted a 3 nm blue-shift in the emission upon binding of a single water molecule to the benzothiolate oxygen, while the emission red-shifted by 8 nm for water binding to the thiazole oxygen. In other work,[28] Song and Rhee calculated the average emission energies (RI-CIS(D) without EOM-CCSD corrections) for solvated oxyluciferin ion configurations that had one more water on the thiazole oxygen than on the benzothiazole oxygen (1.419 eV), the same number on both oxygens (1.429 eV), and one more on the benzothiazole oxygen than on the thiazole oxygen (1.449 eV). Even though the trends from these two works are in accordance with our reasoning, the shifts are small. Song and Rhee instead ascribed color modulation to nearby charges, for example, the positively charged ammonium of a protonated lysine residue or the negatively charged AMP.

An analysis of energetic interactions within the luciferase active site by Milne et al. using the fragment molecular orbital method supports the importance of both the charged species and the active site water molecules in terms of their (de)stabilizing effects on the oxyluciferin anion in the ground state.[27] However, because the theoretical models commonly employed in this field of research in general appear to underestimate the blue-shift in absorption by a single water molecule, the influence on emission may also be underestimated. More work is clearly needed to fully address the role of the nearby environment in fine-tuning the details of the electronic transition between the ground and excited states of this system.

■ CONCLUSION

The action spectra reported here provide the first experimental evidence on the absorption by the singly charged oxyluciferinate anion and its complex with water isolated in vacuo and demonstrated a strong perturbation of the electronic structure by a single water molecule. A range of calculations using methods of varying theoretical complexity uniformly support the experimental data and were found to provide reliable predictions of color-shifts in the $[(\mathbf{OxyLH})(\mathbf{H_2O})]^-$ and $\mathbf{DMOxyL}^-$ systems, although the magnitude of the shifts was underestimated. We cannot from our absorption experiments tell the exact role of a water molecule on the emission but only speculate that its influence is large enough for color modulation because it significantly perturbs the difference in energy levels between ground and excited states when it binds to the ground-state geometry. Obtaining quantitative agreement with experiment from calculations on these ions is nontrivial, and more work is needed to improve the theoretical description. Importantly, for a theoretical model to be used to shed light on microenvironmental effects in firefly luminescence, it is required to provide the experimentally measured energy difference between the ground and excited states of the bare oxyluciferinate anion and the perturbation caused by a water molecule bound to the ground-state geometry.

■ METHODS

Experimental Details. The setups used for gas-phase spectroscopy have been described in detail elsewhere,[30−36,40,41] and only a brief description is given below. Oxyluciferin and 5,5-dimethyloxyluciferin, prepared as described before,[14] were dissolved in methanol and electrosprayed. Ions were accumulated in a multipole ion trap in which they experienced collisions with helium buffer gas kept at room temperature.

In the ELISA experiments, an ion bunch was accelerated to kinetic energy of 22 keV, and the ions of interest were selected with a bending magnet. These were injected into the ring that is based on purely electrostatic deflectors and focusing elements. The ions circulated until they changed their mass-to-charge ratio as a result of either collisions with residual gas in the ring (pressure of about 10^{-10} mbar) or photoexcitation. Neutrals produced on the injection side of the ring were not influenced by the electric fields and hit a microchannel plate detector located at the end of the straight section. The rate of neutrals hitting the detector was a measure of the number of ions circulating in the ring. $\mathbf{OxyLH}^-$ ions were photoexcited after about 45 ms. The third harmonic (355 nm) from a Nd:YAG laser was used to pump an optical parametric oscillator (OPO) (EKSPLA laser system). Neutral density filters were used to attenuate the laser power. The repetition rate of the experiment was 10 Hz.

dx.doi.org/10.1021/ja311400t | J. Am. Chem. Soc. 2013, 135, 6485−6493

For experiments using the accelerator mass spectrometer, an ion bunch was accelerated to energy of 50 keV, and appropriate ions were again selected with a bending magnet. These were photoexcited by light from a laser system similar to that used with ELISA in a merged beam configuration. An electrostatic analyzer allowed particular fragment ions to reach a channeltron detector where they were counted. The yield of fragment ions as a function of excitation wavelength was monitored up to 3 μs after photoexcitation. The experiment was performed at a repetition rate of 40 Hz. The laser was run at 20 Hz; thus only every second ion bunch was irradiated to obtain the real laser-induced signal. Also, laser-off spectra were used to correct for ion beam fluctuations from the yield of fragment ions produced as a result of collisions with the residual gas. Hydrated ions were generated by introducing water vapor in an octopole transmission guide located before the multipole trap. The kinetic energies of the ions in the ion source were retained as low as possible to prevent collision-induced water loss from the fragile molecular complexes. The ion beam signal of the complexes was insufficient for meaningful corrections for ion beam fluctuations; instead, the experiment was repeated multiple times to compensate for such variations.

Theoretical Methods. All electronic structure calculations were performed using GAMESS-US (1 October 2010 (R1) release).[42]

Geometries were optimized at the B3LYP[43] level with the diffuse-augmented polarized double-ζ basis set Def2-SVPD.[44] The isolated anion was optimized in both the cis and the trans conformations because both might be populated in the experiment. An energy difference of 23.6 kJ mol^{-1} was found, indicating a Boltzmann factor ratio of 1: 5.14×10^{-5} in favor of the trans-form at 300 K, and so the cis-form was neglected thereafter. That the trans-enol form of **OxyLH**$^-$ might be important was also considered, but this geometry was found to lie 47.4 kJ mol^{-1} higher than the trans-keto form (Boltzmann ratio of 1:5.97×10^{-9} in favor of the keto-form). *trans*-**DMOxyL**$^-$ was optimized at the same level.

Geometry optimizations for the $[(\mathbf{OxyLH})(\mathbf{H_2O})]^-$ complex were performed with water hydrogen-bonded to either the benzothiazole or the thiazolone end of the trans-keto anion. The thiazolone-bound configuration lay 10.5 kJ mol^{-1} higher in energy with a corresponding Boltzmann factor ratio of 1:1.48×10^{-2} favoring the benzothiazole complex at 300 K and indicating an insignificant contribution from the thiazolone configuration.

To obtain a computational benchmark for the electronic excitations in these systems, calculations were performed with equation-of-motion coupled cluster theory including single and double excitations (EOM-CCSD).[38,45−48] The inclusion of triples excitations for molecules of this size was too demanding, and therefore the calculations were truncated at the EOM-CCSD level. However, the results obtained showed that the excitations were predominantly single-electron in character meaning that the physics required to accurately describe these excitations was already contained in the EOM-CCSD method.[38] Both the Def2-SVPD and the large Def2-TZVPPD basis sets were used. To minimize the computational effort involved in these calculations in terms of memory- and disk-usage, the reduced virtual space method[49] was employed. A cutoff of 50 eV above the HOMO level was found to give results that changed by less than 2 nm when the cutoff was increased to 60 eV and by less than 1 nm when increased to 70 eV. These changes were not consistently positive or negative, due to the nonvariational nature of the calculations, and so negligible net change was seen beyond the 50 eV cutoff.

TDDFT[50] calculations used a series of four functional forms of increasing formal complexity representing different rungs on the Jacob's ladder of (TD)DFT approximations.[51−53] The SVWN (local density approximation) and BLYP (generalized gradient approximation) functionals were selected to investigate the performance of pure DFT in this system.[54−56] The commonly used hybrid functional B3LYP (20% Hartree−Fock (HF) exchange) was also included. For excitations with significant nonlocal character, TDDFT methods can produce large errors due to an incomplete treatment of long-range interactions.[57,58] The range-separated hybrid CAM-B3LYP functional, designed to provide a more balanced description of excitation processes with, for example, charge-transfer character,[59] was therefore also included. TDDFT calculations were performed with the Def2-SVPD basis set and repeated with the much more flexible Def2-TZVPPD basis.[44] Minor changes (~0.01 eV) indicated that the Def2-SVPD results were well converged.

Molecular dynamics simulations were performed with Tinker v6.1.[60] **OxyLH**$^-$ parameters[24] were converted to fit the Tinker CHARMM22[61,62] functional form. Torsional parameters relating to the bond bridging the two heterocylic substructures were adjusted for a better fit of the torsion profile calculated with DFT (see the Supporting Information). Additional parameters required for **DMOxyL**$^-$ and $[(\mathbf{OxyLH})(\mathbf{H_2O})]^-$ were taken from the CHARMM22 set. Atomic partial charges were calculated using the CHELPG approach (charges from electrostatic potentials using a grid-based method)[63] at the B3LYP/Def2-SVPD level with Orca v2.9.0.[64] 300 ps in vacuo simulations were run at 300 K in the NVE ensemble. Sampling at 1 ps intervals gave 300 input structures for subsequent TDDFT/Def2-SVPD calculations using the LDA (SVWN) and CAM-B3LYP functionals. The dominant first excitations and oscillator strengths from each calculation were collected, and a Lorentzian broadening function with a half-width of 10 nm was applied using the Gabedit v2.4.0 package.[65] The resulting composite peaks were then renormalized so as to fit them onto the same scale as the individual excitations.

■ ASSOCIATED CONTENT

Ⓢ Supporting Information

Force field parameters used in molecular dynamics simulations of the oxyluciferinate and 5,5-dimethyloxyluciferinate anions. B3LYP/Def2-SVPD optimized geometries (and total energies) used in EOM-CCSD and TDDFT single-point calculations. This material is available free of charge via the Internet at http://pubs.acs.org.

■ AUTHOR INFORMATION

Corresponding Author

sbn@phys.au.dk; pance.naumov@nyu.edu; bruce@teor.fis.uc.pt

Notes

The authors declare no competing financial interest.

■ ACKNOWLEDGMENTS

S.B.N. gratefully acknowledges support from Lundbeckfonden. P.N. thanks the Human Frontier Science Project (grant RGY0081/2011) and the Kyoto University's Hakubi Project for funding. B.F.M. thanks the Portuguese Foundation for Science and Technology for funding (PTDC/FIS/103587/2008) and the Laboratory for Advanced Computation of the University of Coimbra for the provision of computer resources, technical support, and assistance. P.N. acknowledges financial support from the Swedish Research Council (Grant No. 621-2010-5014). M.L. thanks SERC (Swedish e-Science Research Center) for funding and SNIC for providing computer resources.

■ REFERENCES

(1) Shimomura, O. *Bioluminescence: Chemical Principles and Methods*; World Scientific: NJ, 2006.

(2) Cormier, M. J.; Hori, K.; Anderson, J. M. *Biochim. Biophys. Acta* **1974**, *346*, 137−164.

(3) Liu, F.; Liu, Y.; De Vico, L.; Lindh, R. *J. Am. Chem. Soc.* **2009**, *131*, 6181−6188.

(4) Ando, Y.; Niwa, K.; Yamada, N.; Enomoto, T.; Irie, T.; Kubota, H.; Ohmiya, Y.; Akiyama, H. *Nat. Photonics* **2008**, *2*, 44−47.

(5) Kricka, L. J. *Biolumin. Chemilumin., Part C: Methods Enzymol.* **2000**, *305*, 333−345.

(6) Greer, L. F.; Szalay, A. A. *Luminescence* **2002**, *17*, 43−74.

(7) Mezzanotte, L.; Que, I.; Kaijzel, E.; Branchini, B.; Roda, A.; Löwik, C. *PLoS One* **2011**, *6*, e19277.
(8) Foucault, M.-L.; Thomas, L.; Goussard, S.; Branchini, B. R.; Grillot-Courvalin, C. *Appl. Environ. Microbiol.* **2010**, *76*, 264−274.
(9) Takakura, H.; Sasakura, K.; Ueno, T.; Urano, Y.; Terai, T.; Hanaoka, K.; Tsuboi, T.; Nagano, T. *Chem.-Asian J.* **2010**, *5*, 2053−2061.
(10) So, M.-K.; Xu, C.; Loening, A. M.; Gambhir, S. S.; Rao, J. *Nat. Biotechnol.* **2006**, *24*, 339−343.
(11) Ma, N.; Marshall, A. F.; Rao, J. *J. Am. Chem. Soc.* **2010**, *132*, 6884−6885.
(12) Branchini, B. R.; Rosenberg, J. C.; Ablamsky, D. M.; Taylor, K. P.; Southworth, T. L.; Linder, S. J. *Anal. Biochem.* **2011**, *414*, 239−245.
(13) Solntsev, K. M.; Laptenok, S. P.; Naumov, P. *J. Am. Chem. Soc.* **2012**, *134*, 16452−16455.
(14) Naumov, P.; Ozawa, Y.; Ohkubo, K.; Fukuzumi, S. *J. Am. Chem. Soc.* **2009**, *131*, 11590−11605.
(15) Naumov, P.; Kochunnoonny, M. *J. Am. Chem. Soc.* **2010**, *132*, 11566−11579.
(16) Navizet, I.; Liu, Y.-J.; Ferré, N.; Roca-Sanjuán, D.; Lindh, R. *ChemPhysChem* **2011**, *12*, 3064−3076.
(17) Hosseinkhani, S. *Cell. Mol. Life Sci.* **2011**, *68*, 1167−1182.
(18) Pinto da Silva, L.; Esteves da Silva, J. C. G. *ChemPhysChem* **2011**, *12*, 3002−3008.
(19) Ren, A.; Goddard, J. D. *J. Photochem. Photobiol., B* **2005**, *81*, 163−170.
(20) Min, C.; Zou, L.; Sun, Y.; Guo, J.; Ren, A.-M.; Goddard, J. D. *Chin. J. Chem.* **2011**, *29*, 2301−2307.
(21) Orlova, G.; Goddard, J. D.; Brovko, L. Y. *J. Am. Chem. Soc.* **2003**, *125*, 6962−6971.
(22) Nakatani, N.; Hasegawa, J. Y.; Nakatsuji, H. *J. Am. Chem. Soc.* **2007**, *129*, 8756−8765.
(23) Navizet, I.; Liu, Y.-J.; Ferré, N.; Xiao, H.-Y.; Fang, W.-H.; Lindh, R. *J. Am. Chem. Soc.* **2010**, *132*, 706−712.
(24) Song, C.-I.; Rhee, Y. M. *Int. J. Quantum Chem.* **2011**, *111*, 4091−4105.
(25) Nakatsu, T.; Ichiyama, S.; Hiratake, J.; Saldanha, A.; Kobashi, N.; Sakata, K.; Kato, H. *Nature* **2006**, *440*, 372−376.
(26) Conti, E.; Franks, N.; Brick, P. *Structure* **1996**, *4*, 287−298.
(27) Milne, B. F.; Marques, M. A. L.; Nogueira, F. *Phys. Chem. Chem. Phys.* **2010**, *12*, 14285.
(28) Song, C.-I.; Rhee, Y. M. *J. Am. Chem. Soc.* **2011**, *133*, 12040−12049.
(29) Navizet, I.; Roca-Sanjuán, D.; Yue, L.; Liu, Y.-J.; Ferré, N.; Lindh, R. *Photochem. Photobiol.* **2012**, *89*, 319−3125.
(30) Brøndsted Nielsen, S.; Lapierre, A.; Andersen, J. U.; Pedersen, U. V.; Tomita, S.; Andersen, L. H. *Phys. Rev. Lett.* **2001**, *87*, 228102.
(31) Rajput, J.; Rahbek, D.; Andersen, L.; Hirshfeld, A.; Sheves, M.; Altoè, P.; Orlandi, G.; Garavelli, M. *Angew. Chem., Int. Ed.* **2010**, *49*, 1790−1793.
(32) Lykkegaard, M. K.; Ehlerding, A.; Hvelplund, P.; Kadhane, U.; Kirketerp, M.-B. S.; Brønsted Nielsen, S.; Panja, S.; Wyer, J. A.; Zettergren, H. *J. Am. Chem. Soc.* **2008**, *130*, 11856−11857.
(33) Wyer, J. A.; Brøndsted Nielsen, S. *J. Chem. Phys.* **2010**, *133*, 084306.
(34) Wyer, J. A.; Ehlerding, A.; Zettergren, H.; Kirketerp, M.-B. S.; Brøndsted Nielsen, S. *J. Phys. Chem. A* **2009**, *113*, 9277−9285.
(35) Wyer, J. A.; Jensen, C. S.; Brøndsted Nielsen, S. *Int. J. Mass Spectrom.* **2011**, *308*, 126−132.
(36) Støchkel, K.; Milne, B. F.; Brøndsted Nielsen, S. *J. Phys. Chem. A* **2011**, *115*, 2155−2159.
(37) Gomi, K.; Kajiyama, N. *J. Biol. Chem.* **2001**, *276*, 36508−36513.
(38) Bartlett, R. J. *Wiley Interdiscip. Rev. : Comput. Mol. Sci.* **2012**, *2*, 126−138.
(39) Cai, D.; Marques, M. A. L.; Nogueira, F. *J. Phys. Chem. B* **2011**, *115*, 329−332.
(40) Støchkel, K.; Kadhane, U.; Andersen, J. U.; Holm, A. I. S.; Hvelplund, P.; Kirketerp, M.-B. S.; Larsen, M. K.; Lykkegaard, M. K.; Nielsen, S. B.; Panja, S.; Zettergren, H. *Rev. Sci. Instrum.* **2008**, *79*, 023107−023107-6.
(41) Andersen, J. U.; Hvelplund, P.; Nielsen, S. B.; Tomita, S.; Wahlgreen, H.; Møller, S. P.; Pedersen, U. V.; Forster, J. S.; Jørgensen, T. J. D. *Rev. Sci. Instrum.* **2002**, *73*, 1284.
(42) Schmidt, M. W.; Baldridge, K. K.; Boatz, J. A.; Elbert, S. T.; Gordon, M. S.; Jensen, J. H.; Koseki, S.; Matsunaga, N.; Nguyen, K. A.; Su, S. J.; Windus, T. L.; Dupuis, M.; Montgomery, J. A. *J. Comput. Chem.* **1993**, *14*, 1347−1363.
(43) Stephens, P. J.; Devlin, F. J.; Chabalowski, C. F.; Frisch, M. J. *J. Phys. Chem.* **1994**, *98*, 11623−11627.
(44) Rappoport, D.; Furche, F. *J. Chem. Phys.* **2010**, *133*, 134105.
(45) Stanton, J. F.; Bartlett, R. J. *J. Chem. Phys.* **1993**, *98*, 7029−7039.
(46) Piecuch, P.; Kucharski, S. A.; Kowalski, K.; Musial, M. *Comput. Phys. Commun.* **2002**, *149*, 71−96.
(47) Kowalski, K.; Piecuch, P. *J. Chem. Phys.* **2004**, *120*, 1715−1738.
(48) Wloch, M.; Gour, J. R.; Kowalski, K.; Piecuch, P. *J. Chem. Phys.* **2005**, *122*, 214107.
(49) Send, R.; Kaila, V. R. I.; Sundholm, D. *J. Chem. Phys.* **2011**, *134*, 214114.
(50) Runge, E.; Gross, E. K. U. *Phys. Rev. Lett.* **1984**, *52*, 997.
(51) Perdew, J. P.; Schmidt, K. *AIP Conf. Proc.* **2001**, *577*, 1−20.
(52) Perdew, J. P.; Ruzsinszky, A.; Constantin, L. A.; Sun, J.; Csonka, G. I. *J. Chem. Theory Comput.* **2009**, *5*, 902−908.
(53) Casida, M. E. *J. Mol. Struct. (THEOCHEM)* **2009**, *914*, 3−18.
(54) Vosko, S.; Wilk, L.; Nusair, M. *Can. J. Phys.* **1980**, *58*, 1200−1211.
(55) Becke, A. *Phys. Rev. A* **1988**, *38*, 3098−3100.
(56) Lee, C.; Yang, W.; Parr, R. *Phys. Rev. B* **1988**, *37*, 785−789.
(57) Peach, M. J. G.; Benfield, P.; Helgaker, T.; Tozer, D. J. *J. Chem. Phys.* **2008**, *128*, 044118.
(58) Peach, M. J. G.; Le Sueur, C. R.; Ruud, K.; Guillaume, M.; Tozer, D. J. *Phys. Chem. Chem. Phys.* **2009**, *11*, 4465−4470.
(59) Yanai, T.; Tew, D. P.; Handy, N. C. *Chem. Phys. Lett.* **2004**, *393*, 51−57.
(60) Ponder, J. W.; Richards, F. M. *J. Comput. Chem.* **1987**, *8*, 1016−1024.
(61) MacKerell, A. D.; et al. *J. Phys. Chem. B* **1998**, *102*, 3586−3616.
(62) Foloppe, N.; MacKerell, A. D., Jr. *J. Comput. Chem.* **2000**, *21*, 86−104.
(63) Breneman, C. M.; Wiberg, K. B. *J. Comput. Chem.* **1990**, *11*, 361−373.
(64) Neese, F. *ORCA, an ab initio, Density Functional and Semiempirical program package*; University of Bonn: Germany, 2006.
(65) Allouche, A.-R. *J. Comput. Chem.* **2011**, *32*, 174−182.